Int J CARS
DOI 10.1007/s11548-008-0242-5

ORIGINAL ARTICLE

# Development and preliminary evaluation of software for planning selective liver embolizations from three-dimensional rotational fluoroscopy imaging

**Eric Pichon · Gyorgy Bekes · Frederic Deschamps · Stephen B. Solomon**

Received: 10 January 2008 / Accepted: 4 June 2008


**Abstract**
*Purpose* Liver cancer can be treated by transcatheter hepatic arterial embolization. Selective embolizations are desirable as they impact tumors and with limited damage to the surrounding healthy liver. These interventions are typically performed under fluoroscopy guidance. The advent of modern C-arms allows for the acquisition of three-dimensional images that offer a very detailed, unambiguous view of the hepatic arterial network.
*Methods* We developed a software specifically for planning selective liver tumor embolization from three-dimensional fluoroscopy. Based on the geometry of the vasculature around a targeted tumor, feeding vessels are inferred and highlighted. This accelerates and simplifies the determination of selective treatment points.
*Results* A retrospective study on nine patients (15 tumors) in two centers showed that the proposed software detected 89% of tumor feeding vessels (unaided radiologists detected 69% based on two-dimensional fluoroscopy) with a positive predictive value of 94% (90% for radiologists). Processing time was 142 s.
*Conclusion* The current report describes a feasibility analysis of a treatment planning software specifically geared to selective transcatheter delivery procedures in interventional oncology. This software takes advantage of recent advances in three-dimensional rotational angiography and vascular segmentation algorithms. It is likely that in the near term these types of tools will become integral parts of transcatheter therapies.

**Keywords** Interventional radiology · Liver · Tumor · Embolization · Planning · Three-dimensional fluoroscopy

E. Pichon (✉)
GE Healthcare, Clinical Software Engineering, Buc, France
e-mail: Eric.Pichon@ge.com

G. Bekes
GE Healthcare, Clinical Software Engineering, Szeged, Hungary

F. Deschamps
Institut Gustave Roussy, Villejuif, France

S. B. Solomon
Memorial Sloan-Kettering Cancer Center, New York, NY, USA

## Introduction

Primary liver cancer (hepatocellular carcinoma) is responsible for about 600,000 deaths per year in the world, 15,000 in the USA alone. Liver tumors can also be metastasis of colorectal cancer (650,000 deaths per year in the world, 50,000 in the USA) or other cancers, see [1,2]. Many liver cancer patients are not good surgical candidates and, over the last few years, several alternative, less invasive, image-guided therapeutic strategies have been developed [3].

For patients that are deemed inoperable, transcatheter hepatic arterial embolization is one such treatment. It is based on the selective catheterization and then embolization of the target tumor vessels. Selectivity is important to minimize toxicity to healthy tissues [4,5]. However, while selectivity is important, it is also critical that the entire tumor be targeted and that "over-selective" catheterization does not lead to exclusion of tumor vessels.

Two-dimensional fluoroscopy has long been the modality of choice for hepatic arterial therapy guidance [6]. The challenge with two-dimensional fluoroscopy is that the hepatic vessels can overlap one another on the two-dimensional display. This can lead to either overly selective or insufficiently selective catheterization. This is addressed by the use of modern interventional C-arms that can perform rotational

angiography and acquire three-dimensional vascular and soft-tissue images [7].

Extracting information from such images can be complex and time consuming. In particular, in the case of selective embolizations, it is necessary to carefully analyze the three-dimensional geometry of all the smallest vessels surrounding the tumor in order to determine what portion of the tumor or of the healthy parenchyma each of the numerous small vessels feed.

In this paper we present a software for planning selective liver embolizations from intra-procedural three-dimensional rotational fluoroscopy imagery. An algorithm for segmenting the arterial tree and determining the portion of the liver that is proximal or distal to any given region of the liver (i.e., what path to follow in order to access a particular vessel and what region of the liver would be impacted if it were to be embolized) will be presented in "Materials and methods". Implementation details will be provided in "Results". Finally, initial validation results, both technical and clinical will be discussed in "Discussion".

## Materials and methods

In this section we propose a general vision for medical procedure planning ("Vision") and introduce the algorithm ("Principle") before formalizing it mathematically ("Formalization") and summarizing the entire workflow ("Workflow").

### Vision

The ultimate planning tool would be a "digital ghost" that would reproduce all properties (e.g., mechanical, chemical, physiological) of the actual patient. This virtual patient would be built using all available patient information (e.g., pre- and intra-procedural imagery, tests results, patient demographics). Several therapeutic strategies could be simulated on the virtual patient. The optimal intervention could then be rehearsed as many times as desired before it is performed on the actual patient.

While this framework exceeds current technology, it can serve as a guiding vision for planning tools. In the case of liver embolization planning, the objective would be to let the user place the tip of a "digital catheter" inside some vessel and simulate injection in order to observe what region of the liver is impacted. Thus the software would determine the region that is distal to a particular point. Conversely, determining what part of the liver is proximal to the region of interest would guide the catheter to the region of interest (see Fig. 1).

For a user-defined region, the objective is thus to determine:

- What is the portion of the arterial tree that is proximal to that region? In other words, what are the vessels that are feeding that region? This information will be useful for determining where to navigate the catheter as well as the where to position the tip of the catheter when injecting the embolizing agent.
- What is the portion of the arterial tree that is distal to the selected embolization points? What region of healthy parenchyma or tumor does it feed? This information will be useful to determine if a considered embolization point (i.e., position of the catheter tip during embolization) might result in over- or under-selective treatment (in which case a new treatment point could be tested proximally or distally).

### Principle

Assume that an initial "vessels versus parenchyma" classification is available for each voxel. This classification needs not be very accurate. In practice, three-dimensional fluoroscopy images are acquired while contrast is injected intra-arterially and a basic thresholding will suffice.

Now imagine that particles are released at the root of the hepatic artery and that their speed $V$ locally depends on the previous classification. Particles can move fast through voxels that have been identified as vessels while they have to move slow in voxels that have been classified as non-vessels. These virtual particles receive no direct physical interpretation. Thus they need not behave in a physically plausible way. For example, they are allowed to extravasate from vascular structures into the parenchyma. The purpose of this framework is to capture the three-dimensional geometry of the problem rather than simulate its physical properties.

Thus the entire liver (vessels and parenchyma) is traversed by a directed flux of particles originating from the entrance of the hepatic artery. If an infinity of virtual particles are released at time $T = 0$, any voxel $p$ within the liver will eventually be reached at some time $T(p)$. The first particle to reach $p$ will have followed a path $\prod(p)$ that is optimal as defined by the local speeds imposed by the model.

In order to develop some intuition, one can think of these optimal paths $\prod(p)$ as the actual trajectory of arterial blood from the entrance in the liver to voxel $p$ (however, it is important to keep in mind that we are not concerned here with an accurate physical simulation).

Considering optimal paths in the entire liver, one can ask:

- which are those that correspond to high local speed values?
- which are those that correspond to low local speed values?

The answers to these questions can be used to improve the initial vessel/non-vessel classification. Real vessel voxels will be optimally reached from the seed point $S$ by following the high speed path that corresponds to the actual arterial network. Wrongly classified vessel voxels that are isolated in the liver parenchyma will not be reachable through such

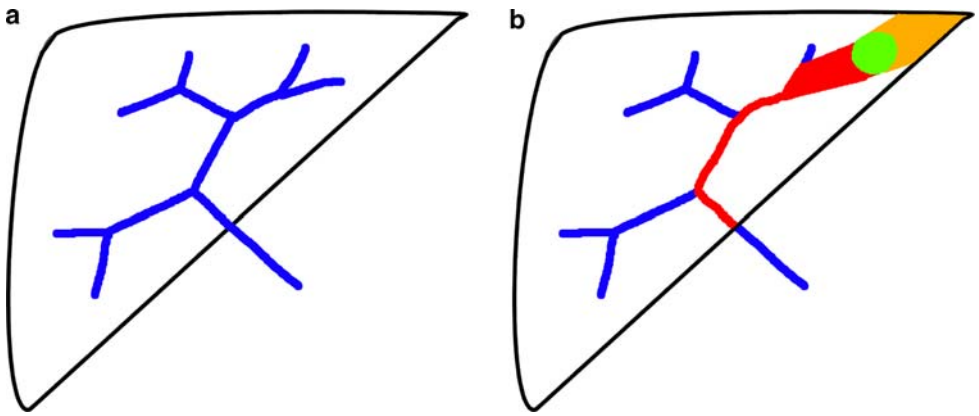


**Fig. 1** **a** Schematic diagram of the liver parenchyma and hepatic arterial tree. **b** User-define region of interest (*green*) and corresponding proximal (*red*) and distal (*orange*) regions

a favorable path. By integrating information along optimal paths that correspond by construction to the actual vessels to be detected, the algorithm can actually improve the initial classification.

Considering optimal paths that traverse a given region $R$, one can ask:

- what region of the liver did they traverse before reaching $R$?
- what region of the liver will they traverse after reaching $R$?

The answer to these questions can be used to infer what are the vessels that feed region $R$ and what is the region that would be impacted if irrigation would cease to $R$ (see Fig. 1).

## Formalization

In this section we provide a more formal mathematical review of the algorithm. Overall three-dimensional rotational angiographic imaging is used to define the speed at which virtual particles will flow out of a user prescribed seed-point. Analyzing the behavior of these particles allows for the automatic determination of the vascular structures. Background material can be found in [8].

Let's consider that some liver mask $L$ is available. Based on image information, all voxels within $L$ can be fuzzily classified as either vessel or non-vessel. This takes the form of a scalar field:

$$C : L \rightarrow [0, 1] \tag{1}$$

where $C$ denotes the chance of voxels within $L$ to be within a vessel.

Define particle speed as some increasing function of $C$: particles can move fast inside vessels and slow in the parenchyma:

$$V : L \rightarrow ]0, +\infty[ \tag{2}$$

This prescribes the speed a virtual particle will travel at any given point. This speed should be strictly positive everywhere lest particles get trapped at a given location. Strictly positive, increasing functions of $C$ can be used.

Assume that we have a seed region $S \subset L$. Define the arrival time map as the minimum time needed for reaching a voxel $p$ from $S$ subject to the speed constraints $V$:

$$T : L \rightarrow [0, +\infty[ \tag{3}$$

is the solution of the Eikonal equation:

$$\begin{cases} |\nabla T| = 1/V & \text{on} \quad L \backslash S \\ T = 0 & \text{on} \quad S \end{cases} \tag{4}$$

In order to understand Eq. (4), consider a particle moving from $x$ to $x + dx$. Since it will be prescribed to move with speed $V(x)$, arrival times will be such that: $T(x + dx) - T(x) = |\mathrm{dx}|/V(x)$. Consider now a first order development of the arrival time map $T$ at $x$: $T(x+dx)-T(x) = \nabla T(x)dx$. Equation (4) can be obtained by combining these two relations. For more mathematical details, see [8].

Now, consider a region $R$ and consider the solution $E_R$ of the transport equation:

$$\begin{cases} \nabla E_R \cdot \frac{\nabla T}{|\nabla T|} = 1 & \text{on} \quad L \backslash R \\ E_R = 0 & \text{on} \quad R \end{cases} \tag{5}$$

Positive values of the scalar field $E_R$ at a given voxel $v$ can be interpreted as the Euclidean distance that particles reaching $v$ have traversed since they left $R$. Negative values correspond to the Euclidean distance that particles have to cover before they reach $R$. Zero values correspond to voxels that are either inside $R$ or on a path that does not pass through $R$.

One particular case consists of choosing $R = S$. Since all particles originate from $S$, the scalar field $E_s$ is simply at each voxel the Euclidean distance that particles traveled from $S$. Dividing this field by the arrival time map $T$, one obtains at each voxel the mean particle speed of the path leading to that voxel. By construction, "fast" paths can only be achieved by traversing preferentially voxels that have been classified as vessels. Low values of the ratio $\frac{E_s}{T}$ can be used to

define a vessel mask. Because it will make use of information along the path followed by particles instead of purely local information, this mask will be more robust than the initial vessel classification. For example a speck of high intensity noise that would initially have been erroneously classified as a probable vessel voxel will not be reachable through a path of mostly high intensity voxels. Therefore, while locally particle speed might be high, the average speed on the path reaching this voxel will not be high. This voxel will therefore not be classified as a vessel voxel.

It should be noted that the average speed along the path that a particle follows is not necessarily the best criteria. Consider a non-vessel voxel $p$ that is close to a vessel voxel $q$, both being far away from the initial seed region $S$. The average speeds along optimal paths to $p$ and $q$ cannot be very different because it is possible to reach $p$ by reaching $q$ and then following the slow but short path from $q$ to $p$. Indeed, using the average speed to discriminate between vessel and non-vessel voxels will work best far away from actual voxels. This would not be the case if we had considered the minimum speed along the optimal path instead of the average speed along this path. The difficulty in turn with this approach is that the final classification will be based on only one voxel. For example a very thin vessel might not be properly recovered if image quality is low and it appears slightly discontinuous. Fortunately a compromise can be reached between these two extremes by considering the $n$-norm of local intensities of a path leading to a particular voxel $p$:

$$A_n(p) = \left( \frac{\int_{\prod(p)} V(q)^n}{\int_{\pi(p)1}} \right)^{\frac{1}{n}} \tag{6}$$

One can verify that $n = 1$ corresponds to the average value of the speed $V$ along the path and that as $n \to +\infty$, $A_n(p)$ converges towards the maximum value of $V$ along the optimal path $\prod(p)$.

In summary, as is classical in dynamic programming, optimal paths for an image-defined local speed (based on vessel/non-vessel classification) are determined implicitly by solving for an earliest arrival time scalar field. This provides a flux model inside the liver that can be thought of as a very crude approximation of blood flow and used to determine which part is distal or proximal to a user-supplied region. A slightly different criteria is then used to discriminate between all globally optimal paths those that are more consistently locally optimal. This is used to improve the initial vessel classification.

An extended version of the Fast Marching [8] framework was employed to determine the distance maps. This allowed for the efficient determination of optimal paths. Moreover the algorithm was implemented using the implementation proposed by Yatziv et al. [9].

Workflow

1. Three-dimensional fluoroscopy is acquired and imported (see Fig. 2a)
2. The user clicks at the entrance of the liver. Optimal paths are computed (see "Results" for details, the processing time is $\sim 30$ s), finally the vasculature is displayed (see Fig. 2b)
3. The user determines tumor location using a spherical ROI ($\sim 5$ user clicks, see Fig. 2c)
4. The proximal region is computed (processing time $\sim 10$ s) and displayed (see Fig. 2d). Based on this the user can select embolization putative points.
5. The user clicks on one of the embolization points.
6. The proximal and distal regions are computed (processing time $\sim 30$ s) and displayed (see Fig. 2e, f)
7. If result is satisfactory, store location of embolization point. If not, update location of embolization point and iterate to step 5.

See Fig. 3 for a recapitulation of the workflow.

## Results

### Acquisition

Validation of the proposed technique has been initiated at two clinical sites. A total of nine patients (three in one site and six in the other) who underwent three-dimensional rotational angiography during their hepatic artery tumor embolizations were included retrospectively in this evaluation.

Angiographies were performed with a commercially available angiographic unit (Innova 4100, GE Healthcare, Chalfont St Gilles, UK). For the rotation, patient arms were elevated above their heads. After breathing was suspended, there was a 4 s delay for contrast filling of the vessels and tumors prior to the C-arm rotation. Contrast medium (Omnipaque 300 mgI/ml; GE Healthcare) was injected at a flow rate of 3 cc/s through the microcatheter in the proper hepatic artery. The total contrast used for the rotation was 27 ml. The C-arm rotated 200° around the patient at 40° per second. During rotation 148 images were obtained at a frame rate of 30 frames per second. The reconstructed three-dimensional field of view was $23 \times 23 \times 23$ cm and the image matrix size was $512 \times 512 \times 512$.

### Technical validation

An initial technical study was performed by three experienced radiologists. While this study was performed by medical doctors, it focused on technical rather than clinical aspects. In particular, the study included intra-operator repeatability tests (wherein the same task was performed three times

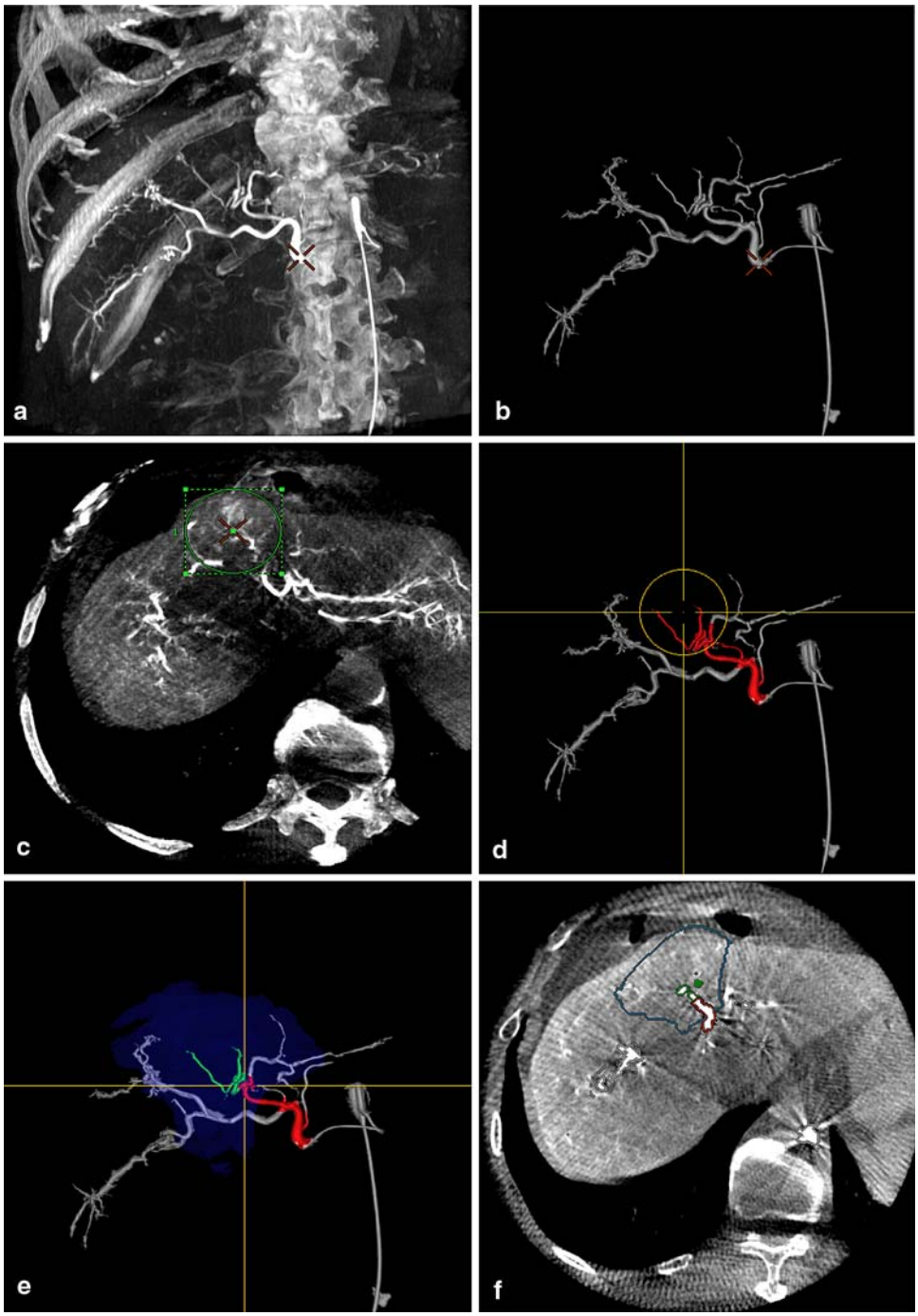


**Fig. 2** **a** MIP rendering of three-dimensional fluoroscopy. **b** Proposed vascular mask. **c** Target region (*green circle*) as determined by user. **d** Corresponding feeding vessels (*red*) as determined by proposed software. **e** Embolization point (*orange cross-hair*) and volume rendering of catheter path (*red*), distal vessels (*green*) and impacted parenchyma (*blue*) as predicted by proposed software. **f** Two-dimensional rendering of catheter path (*red*), distal vessels (*green*) and impacted parenchyma (*blue*) as predicted by proposed software

by the same user) as well as inter-operator reproducibility tests (wherein three users performed the same segmentation tasks).

Inter-operator repeatability

Let $I_1$ and $I_2$ denote two binary segmented volumes and $|\ \ |$ the set cardinal operator. The reproducibility metric was defined as:

$$M_{\text{overlap}} = \frac{|I_1 \cap I_2|}{|I_1 \cup I_2|} \times 100 \tag{7}$$

Users were instructed to select seed points at the beginning of the catheter. The overall reproducibility for vascular masks was is 92.5% with a standard deviation of 7.37%.

Intra-operator repeatability

The same user repeatedly selected seed points anywhere between the beginning of the catheter and the proper hepatic

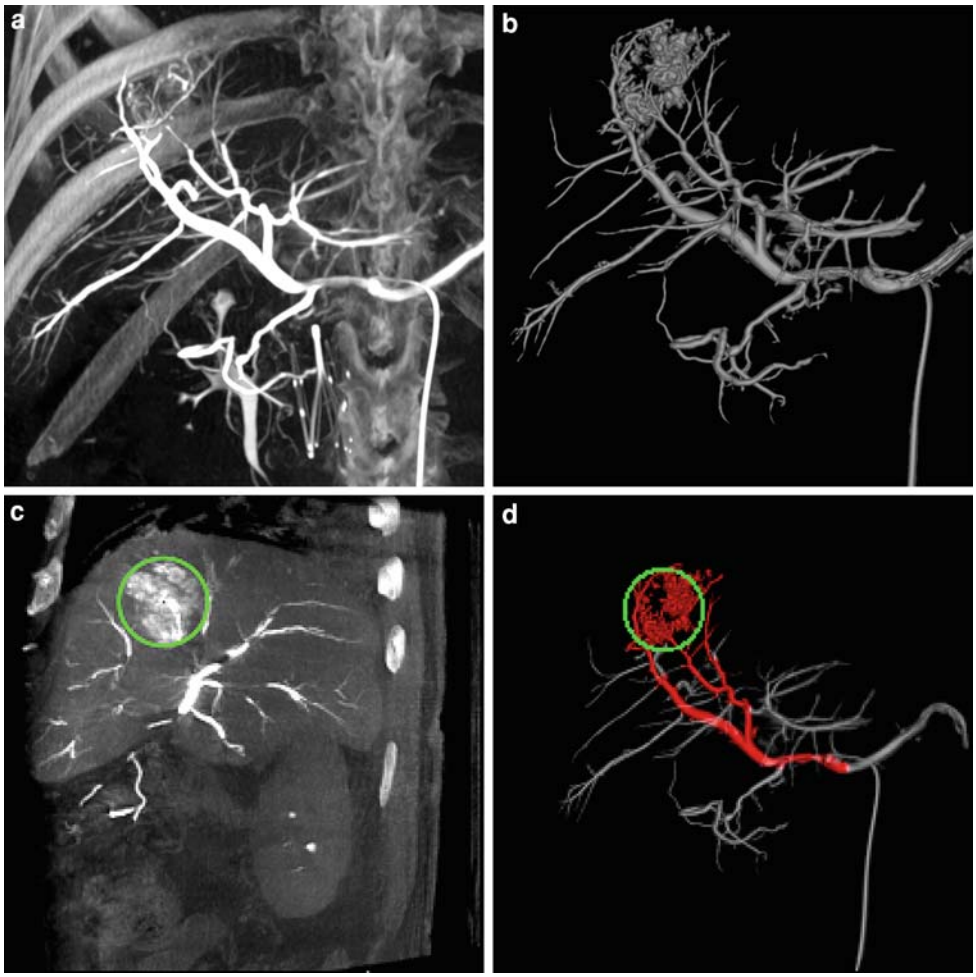


**Fig. 3** Screenshots of proposed software. Initial three-dimensional fluoroscopy image (*top left*), segmented vascular tree (*top right*), manual tumor definition (*green*, *bottom left*) and computed feeding vessels (*red*, *bottom right*)

artery. The overall reproducibility repeatability value was 88.95% with a standard deviation of 8.27%.

### Clinical evaluation

In order to validate the algorithm, a separate study was performed. At each site, one experienced radiologist determined *a posteriori* vessel-feeding vessels on series of three and six consecutive patients undergoing selective liver embolizations (six and nine tumors, respectively). This task was performed with great detail (requiring between 10 min and 1 h per case) and using all available information (pre-operative imagery together with all three-dimensional and two-dimensional sequences acquired during the case). This constituted the ground-truth.

Two other radiologists were then asked to determine the same tumor feeding vessels. In order to simulate an interventional context, the task had to be completed within a few minutes from the first two-dimensional and three-dimensional images. The proposed software was also applied to the first three-dimensional image. See Table 1 for results. Overall the proposed system proved slightly faster and more selective than unaided radiologists. Sensitivity was significantly improved with the software determining 89% versus 69% for radiologists.

## Discussion

### Related work

Wu et al. [10] have discussed how a physically realistic "virtual dummy" can be built for training users on some catheter-based procedures. Their technique relies on simulating fluid propagation inside the vessels using a simplified version of the Navier–Stokes equations. While it could be used for planning, adapting their physics-based model to the anatomy of a particular patient is computationally expensive and might not be compatible with the strict time constraints of an actual intervention. In contrast, the technique we propose is not physics-based but has the advantage of being much simpler and more efficiently implementable.

**Table 1** Determination of tumor-feeding vessel: proposed software versus radiologists ($N = 15$ tumors)

| | Radiologists | Software |
|---|---|---|
| Sensitivity (%) | 69 | 89 |
| Positive predictive value (%) | 90 | 94 |
| Time (s) | 165 | 142 |

Selle et al. [11] have proposed software techniques for planning liver surgery. While the end goal is very different, they show that Couinaud segments can be approximated quite efficiently using vascular geometry. Couinaud segments are defined as the regions of the liver irrigated by the 3rd generation branches of the portal vein. In this region of the liver, the portal vein and the hepatic artery run along each other and therefore share the same geometry. Determining Couinaud segments is therefore solving a particular instance of the distal region determination. The technique proposed by Selle et al. is based on Euclidean distance maps. It is therefore mathematically very similar to the proposed technique which makes use of weighted distance maps (i.e., Riemannian instead of Euclidean distances). Their results have been experimentally validated using a corrosion cast on actual human livers (see [11] for details). This proves that, crude geometry-based, non-physical models can be sufficient to capture irrigation patterns in the liver.

Moreover the technique proposed here does not rely on a prior explicit vessel segmentation step. Instead, the entire region of interest, in our case the entire liver is processed and one of the outputs is the separation of the vascular tree from the surrounding parenchyma. This reduces the number of error-prone sequential steps.

### Technical validation

Most of the differences occurred on the boundary of the vessels. While the metric was defined on binary vascular masks, the information is presented to the users in the form of Volume Renderings that are remarkably forgiving to these minor segmentation defects. Another source of differences are very distal portions of the arterial tree that cannot be used for catheter navigation.

### Clinical validation

The software outperformed the radiologists principally on the most distal parts of the vascular structures. When determining the ground truth, a deliberate focus had been put on hyper-selectivity. Some of the radiologists erroneous answers might have resulted in the same treatment point if a less selective strategy had been adopted. Moreover, tt should be noted that the radiologists' score would probably have improved if they could have performed exploratory selective injections.

The proposed technique missed some vessels, in particular some that were small and/or distal. Another improvement area is the differentiation between tumoral blush and vascular structures.

The study has its limitations in that the validation of the software is made on a small number of retrospectively analyzed patients, and the concept of "ground truth" may be flawed. Additionally, while the current study provided a useful method to retrospectively determine the suspected arterial supply to a tumor, it has some inherent limitations in that it does not duplicate the real-life iterative angiographic decision-making that often occurs in practice.

More fundamentally, any rotational angiography treatment planning system will have other limitations. Since the input data originates from the rotational angiogram, vessels not injected will not be depicted. Therefore, if the tumor is supplied by vessels arising from arteries other than the one catheterized, it will not be identified from a proper hepatic injection and will therefore go unrecognized by the proposed software. Perhaps future integration with pre-planning CT angiography studies could help identify extrahepatic or variant vessels prior to the procedure and mitigate this potential software limitation. Also, any treatment planning system will require some processing time. Since analysis of the rotational data will take place while the liver is catheterized, there is time pressure for any practical treatment planning system. The proposed system has the potential to provide this analysis within minutes.

## Conclusion

A software was presented for planning liver embolization from three-dimensional fluoroscopy imagery. Based on a non-physical geometry-based model, the portion of the vasculature that feed a given region of the liver can be estimated together with the portion of the liver that is fed by a particular vessel. The proposed algorithm was efficiently implemented. A case can be processed in a few minutes which appears to be compatible with a real-time interventional context. Initial validation results are very encouraging.

Further validation is underway, in particular to assess the clinical benefits of the proposed technique over standard two-dimensional and three-dimensional fluoroscopy. Other areas

of investigation include the application to hepatic arterial infusion as well as dose quantification.

**Acknowledgments** The authors would like to sincerely thank, Yves Trousset, Michel Grimaud, Marta Fidrich, Laszlo Rusko, Thomas Deschamps (GE Healthcare), Thierry de Baere, Pramod Rao, Antoine Hakime (IGR), and the Interventional Radiology Department of the Memorial Sloan-Kettering Cancer Center (MSKCC).

## References

1. Jemal A, Siegel R, Ward E, Hao Y, Xu J, Murray T, Thun MJ (2008) Statistics C. CA Cancer J Clin 58: 71–96
2. World Health Organization, Cancer programme. http://www.who.int/cancer/en/
3. Cancer L National Cancer Institute, http://www.cancer.gov/cancertopics/types/liver/
4. Leung TK, Lee CM, Chen HC (2005) Anatomic and technical skill factor of gastroduodenal complication in post-transarterial embolization for hepatocellular carcinoma: a retrospective study of 280 cases. World J Gastroenterol 11: 1554–1557
5. Lang EK (1997) Reduced systemic toxicity from superselective chemoembolization compared with systemic chemotherapy in patients with high-risk metastatic gestational trophoblastic disease. Cardiovasc Intervent Radiol 20(4):280–284. doi:10.1007/s002709900152
6. Hsieh MY, Chang WY, Wang LY, Chen SC, Chuang WL, Lu S-N, Wu D-K (1992) Treatment of hepatocellular carcinoma by transcatheter arterial chemoembolization and analysis of prognostic factors. Cancer Chemother Pharmacol 31(Supplement 1): S82–S85
7. Liapi E, Hong K, Georgiades CS, Geschwind JF (2005) Three-dimensional rotational angiography: introduction of an adjunctive tool for successful transarterial chemoembolization. J Vasc Interv Radiol 16: 1241–1245
8. Sethian JA (1999) Level set methods and fast marching methods: evolving interfaces in computational geometry, fluid mechanics, computer vision, and materials science, 2nd edn. Cambridge University Press,Cambridge
9. Yatziv L, Bartesaghi A, Sapiro G (2006) O(N) implementation of the fast marching algorithm. J Comput Phys 212(2): 393–399
10. Wu X, Allard J, Cotin S (2007) Real-Time Modeling of Vascular Flow for Angiography Simulation. MICCAI 1: 557–565
11. Selle D, Preim B, Schenk A, Peitgen HO (2002) Analysis of vasculature for liver surgical planning. IEEE Trans Med Imaging 21(11): 1344–1357